ELSEVIER

Materials Science and Engineering A318 (2001) 15–21

MATERIALS SCIENCE & ENGINEERING A

www.elsevier.com/locate/msea

# Microstructure and mechanical properties at $TiC_p$/Ni-alloy interfaces in laser-synthesized coatings

Xiaolei Wu *, Youshi Hong

*State Key Laboratory of Nonlinear Mechanics, Institute of Mechanics, The Chinese Academy of Sciences, 15 ZhongGuanCun Rd., Beijing 100080, People's Republic of China*

Received 5 March 2001; received in revised form 4 April 2001

**Abstract**

Titanium carbide particle ($TiC_p$) reinforced Ni alloy composite coatings were synthesized by laser cladding using a cw 3 kW $CO_2$ laser. Two kinds of coatings were present in terms of $TiC_p$ origins, i.e. undissolved and in situ reacted $TiC_p$, respectively. The former came from the $TiC_p$ pre-coated on the sample, whereas the latter from in situ reaction between titanium and graphite in the molten pool during laser irradiation. Conventional and high-resolution transmission electron microscope observations showed the epitaxial growth of TiC, the precipitation of CrB, and the chemical reaction between Ti and B elements around phase interfaces of undissolved $TiC_p$. The hardness, $H$, and elastic modulus, $E$, were measured by nanoindentation of the matrix near the $TiC_p$ interface. For undissolved $TiC_p$, the loading curve revealed pop-in phenomena caused by the plastic deformation of the crack formation or debounding of $TiC_p$ from the matrix. As for in situ generated $TiC_p$, no pop-in mark appears. On the other hand, in situ reacted $TiC_p$ led to much higher hardness and modulus than that in the case of undissolved $TiC_p$. The coating reinforced by in situ generated $TiC_p$ displayed the highest impact wear resistance at both low and high impact conditions, as compared with coatings with undissolved $TiC_p$ and without $TiC_p$. The impact wear resistance of the coating reinforced by undissolved $TiC_p$ increases at a low impact work but decreases at a high impact work, as compared with the single Ni alloy coating. The degree of wear for the composite coating depends primarily on the debonding removal of $TiC_p$. 

*Keywords:* Laser cladding; Microstructure; MMC; Coating; Mechanical property; Wear

## 1. Introduction

Laser surface cladding of particle reinforced metal matrix composite (MMC) coatings shows high potential for producing the wear resistant surface layers for ambient and high temperature performance [1,2]. The increase in hardness and wear resistance is primarily due to particle reinforcement of the metal matrix and resistance to plastic flow by particle during wear and abrasion. Contributions also come from solidification reaction products such as fine-scale, dendritic and eutectic carbides which form within the metal matrix as a result of melt/carbide interactions, and from phase transformation products such as solid solutions, precipitates, dispersoids, and martensitic phases. The relatively soft and ductile binder metal contributes the toughness necessary for surface engineering applications.

Various types of carbide and binder alloy compositions can be chosen in order to achieve various property requirements. Matthews [3] clad a paste of Hastellite (50% WC and 50% NiCrSiB, all weight percent) pre-placed on a steel substrate and suggested that such a hard facing technique is highly promising for many applications. A SiC powder plus Stellite (CoNiWFeSiC) composite coating was studied by Abbas and West [4] on EN3b steel and showed excellent wear resistance due to enhanced hardness. Ayers et al. [5,6] injected 30–50 vol.% of 100 μm $TiC_p$ into the laser-

* Corresponding author. Tel.: +86-10-62547527; fax: +86-10-62561284.

*E-mail address:* xlwu@cc5.imech.ac.cn (X. Wu).

0921-5093/01/$ - see front matter 
PII: S0921-5093(01)01394-6

melted zone of titanium alloy (Ti6Al4V) and observed an increase in the hardness to about 450 Hv and a decrease in the coefficient of friction. Partial solution of $TiC_p$ occurred during the laser processing, and TiC dendrites formed during solidification. Lei et al. [7] analyzed the microstructure of 30% TiC reinforced Ni-alloy coating and observed that the coating enhanced the abrasive wear resistance. Jasim et al. [8] and Abboud et al. [9] presented details of a functionally graded clad built up by overlapping laser-processed tracks, with a stepwise increase in the proportion of reinforcement.

The microstructure at interfaces between the reinforced particle and matrix crucially affects the mechanical properties of the coating. Most wear failures of MMC coatings are sensitive to the particle–matrix interface. This is because the stress transfers through phase interfaces by a shear mode to realize the strengthening of the coating. The structure around the interfacial of the reinforced particle varies to a high degree in the molten pool. As far as carbides are concerned, such as WC, SiC, and TiC, etc. dissolution to various degree occur in the molten pool and may lead to a re-growth [10]. Kooper et al. [11] pointed out that the fine, re-precipitated particles contribute mainly to the increase in the wear resistance. The chemical reaction also occurs at the phase interface between the particle and binder alloy. Furthermore, the reaction product will undoubtedly have a strong influence upon the interfacial structure and overall properties of the coating [12]. However, few microstructural observations and mechanical property determinations have been performed at phase interfaces. To our knowledge, the mechanical behavior, such as toughness, hardness, and modulus, is poorly understood. In addition, it is noted that the impact wear resistance of the MMC coating is seldom studied [13], as compared with the abrasive and sliding wear. The mechanism of the impact wear is mainly due to the lack of ductility at interfaces where cracks form and grow. Thus, the optimization of toughness and hardness is required especially at phase interfaces between the reinforced particle and the matrix.

More recently, it has been possible to reliably study the property much near the interface by the use of nanoindentation methods [14,15]. The scale of the deformation is much smaller; depths and forces are in the range of a few nm and nN, respectively. The 'nanomethods' exclusively adopt the contact compliance method. Direct imaging of the indentation, while possible, is generally not a viable experimental procedure. In the present work, the microstructure, mechanical properties such as, hardness and modulus, at phase interfaces between the reinforced particle and the matrix, and the impact wear resistance of the coating were studied and are reported.

## 2. Experimental

Commercial 5CrMnMo steel was used as the substrate. The chemical composition of the steel was 0.43C, 1.23Cr, 1.18Mn, 0.23Mo, balance Fe (all wt.%). A powder mixture of 30 vol.% TiC and 70 vol.% Ni base self-fluxing alloy was used as the coating material. The chemical composition of the Ni alloy was 16Cr, 3.5B, 4.5Si, and 0.8C, balance nickel (all wt.%). The Ni alloy particles had an average size of $-280$ mesh and appeared to be spherical, while $TiC_p$ particles were less than 6 μm in size and irregular in shape. $TiC_p$ and polyethylene glycol were used to obtain a pasty mixture. The paste was pre-coated onto the specimen surface by brushing to a thickness of about 0.8 mm.

A 3 kW continuous wave $CO_2$ laser was employed to produce the coating. The parameters varied were the laser power, beam size, and beam scanning speed. The processing parameters were established after a few trial runs. The criteria for determining the optimum quality of the coatings were based on a compromise of highest hardness, best homogeneity, and lowest occurrence of cracks. On the basis of these criteria, the best processing conditions were determined to be as follows: traverse speed for 14 mm $s^{-1}$, beam diameter for 3 mm, and laser power for 2.5 kW. An argon atmosphere was used to protect the molten pool from the surrounding air.

Another kind of $TiC_p$ reinforced Ni-alloy coating was obtained in a manner described in Ref. [16,17], which provided details of this coating synthesis and resulting microstructure. The coating material consisted of a powder mixture of titanium plus graphite (total 30 vol.%) and a Ni-alloy (70 vol.%). The ratio of titanium to carbon powders corresponded to that of stoichiometric TiC. The average size and purity of titanium and graphite powders were $-320$ mesh and $-300$ mesh and 99.9 and 99.99%, respectively. Using this method, $TiC_p$ was introduced into the coating by in situ reaction between titanium and graphite. The in situ generated $TiC_p$ was different from undissolved $TiC_p$ obtained by the above pre-coating method mainly in two aspects. Firstly, the in situ generated $TiC_p$ had submicron size, often much smaller than that of undissolved $TiC_p$. Secondly, it was compatible with the matrix and the phase interface was free from the deleterious precipitation and chemical reaction as well [16].

The morphology, microstructure and phase interface of the coating were observed using a scanning electron microscope (SEM), X-ray diffraction (XRD), analytical transmission electron microscope (ATEM) and high-resolution transmission electron microscope (HRTEM) equipped with EDX.

The mechanical properties near the $TiC_p$–matrix interface were studied using a CMES nanoindentor. This instrument could monitor and record the dynamic load

and displacement during indentation. The load and displacement resolution was 0.3 μN and 0.17 nm, respectively. A berkovich indentor was used. The system was thermally buffered from its surroundings and the room in which it is housed was temperature-controlled to within ± 1°C. Hardness ($H$) and elastic modulus ($E$) were calculated from the load versus displacement data obtained during nanoindentation. Hardness itself was calculated as the nominal stress underneath the indentor at any point in time, i.e. the applied load to the indentor was divided by the projected area. Because the indentor geometry was known, the area was, in practice, calculated directly from measurements of the total depth. The elastic contribution to this depth was subtracted, so that the resulting hardness measurement reflected the resistance of the material to plastic flow only. The relevant equations for the modulus calculation were

$$\frac{1-v_i^2}{E_i}=\frac{1}{E_r}-\frac{1-v_s^2}{E_s}$$

and

$$E_r=\frac{1}{2h_p}\sqrt{\frac{\pi}{\beta}}\left(\frac{dP}{dL}\right).$$

$E$ and $v$ were, respectively, the Young's modulus and Poisson's ratio, with the subscripts i and s referring to the sample and indentor, respectively. The composite modulus, $E_r$, was obtained from the unloading slope ($dP/dL$) and required determination the plastic depth at which unloading begins ($h_p$). $\beta$ is constant. A value of $v_i = 0.31$ was chosen, since this is the Poisson's ratio for the Ni alloy.

The impact wear experiment was performed using an Impact Wear Test Machine. The experimental conditions were as follows: impact work of 0.2 and 3 J, respectively, impact frequency of 120 cycle $min^{-1}$, room temperature of 22 ± 1°C, and relative humidity of 45 ± 5%. The specimen dimension was φ10 mm × 40 mm. Multiple laser tracks were used and the shift between two successive tracks was kept constant. The optimum shift used to ensure a constant thickness coating was determined to be about 30% of the beam diameter. A GCr15 steel, with a compositions of 1.08C, 1.52Cr, balance Fe (all wt.%), was used as the friction counterpart rotated at a speed of 120 rpm. The heat-treatment condition was austenizing at 1153 K for 1 h, oil cooling and tempering at 853 K for 2 h, and its hardness was HRC62. Solid $Al_2O_3$ particles of average size of −380 mesh were used as abrasives. The abrasives were fed into the space between the specimen and the counterpart at a flow rate of 180 g $min^{-1}$. The surface was polished before tests, because after laser clad processing all specimens had surface roughness of at least a few tens of micrometers.

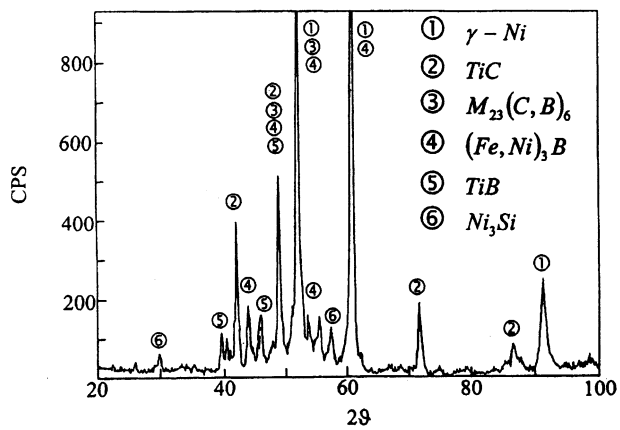


Fig. 1. XRD spectrum of the coating.

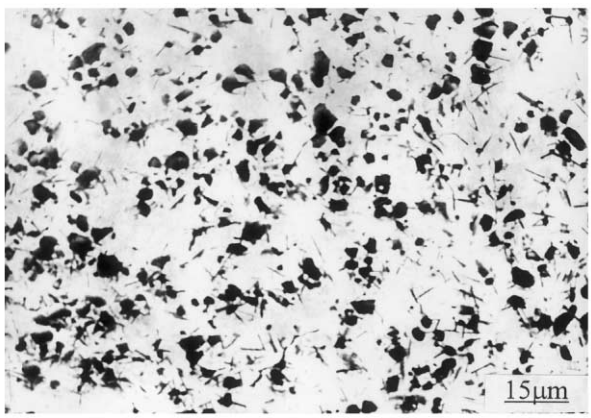


Fig. 2. SEM micrograph showing the coating reinforced by undissolved $TiC_p$.

## 3. Results and discussion

### 3.1. Interfacial structure of undissolved $TiC_p$

Fig. 1 shows the XRD spectrum of the coating reinforced by undissolved $TiC_p$. The main phases consist of TiC, γ-Ni austenite, $(Fe, Cr)_{23}C_6$, $(Fe, Ni)_3B_6$, $Ni_3Si$, and TiB.

Fig. 2 shows the scanning electron micrograph of the cross-section of the coating. It is seen that the undissolved $TiC_p$ is distributed uniformly in the coating.

Fig. 3(a) is a bright-field TEM image showing the interfacial character of the undissolved $TiC_p$. Two kinds of precipitates can be seen. One appears thin loop-like (↑) and the other granular (⇑). Fig. 3(b) is the dark-field TEM image obtained using the diffraction spot (111). It is seen that the loop-like precipitate has the same contrast with $TiC_p$. It is deduced that the loop-like precipitate is TiC grown epitaxially. This is evidence of the partial dissolution of $TiC_p$ on heating and their regrowth on cooling. Fig. 3(c) is the selected area diffraction pattern (SADP) of $TiC_p$ in Fig. 3(a).

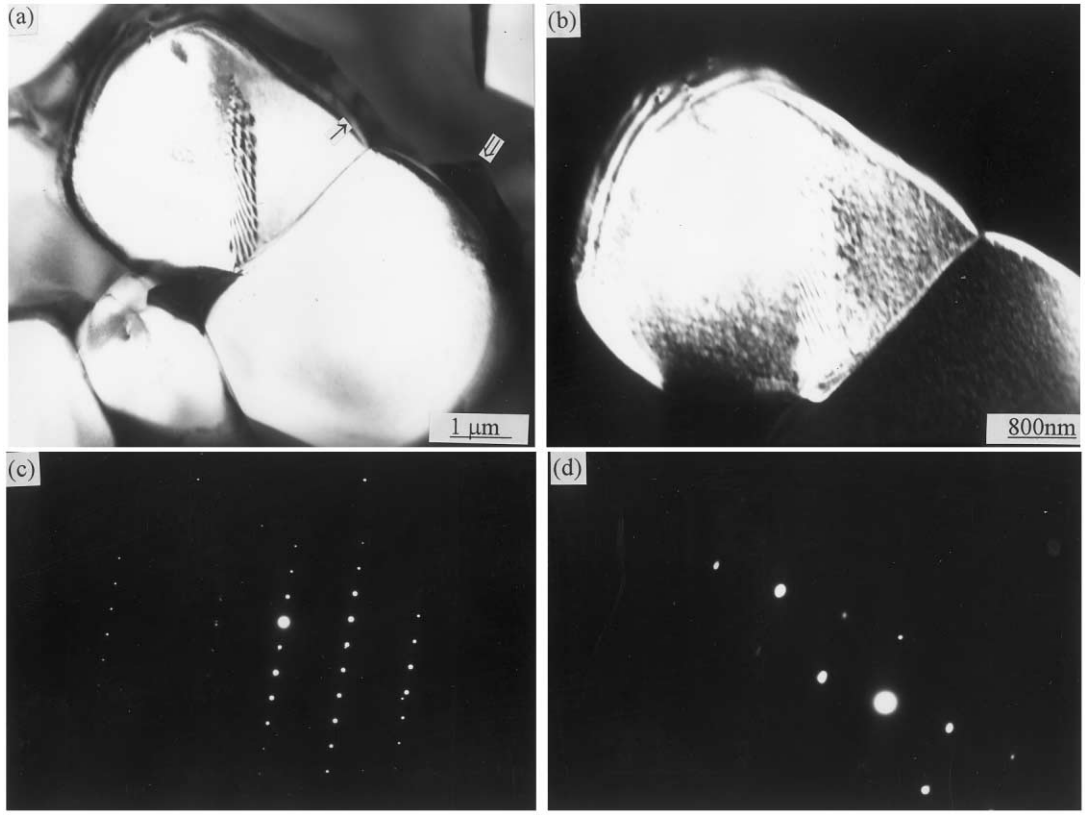


Fig. 3. TEM micrographs: bright-field image showing epitaxial growth of TiC (↑) and precipitation of CrB (⇑) (a), dark-field image of $TiC_p$ (b), SADP of $TiC_p$ (c), SADP of CrB (d).

Fig. 3(d) is SADP from the granular precipitate. It is determined that the granular precipitate is CrB. The nucleation of CrB at interfaces between $TiC_p$ and the matrix is widely observed.

Fig. 4 shows the HRTEM image at interfaces between undissolved $TiC_p$ and the matrix. A thin reaction layer is clearly seen at the edges of the undissolved $TiC_p$. The crystal structure was not determined due to its small size. However, the chemical composition of the layer was analyzed using EDX. It is determined that the layer consists of Ti and B, with the latter ranging from 38 to 63 at.%. Thus, the thin layer formation is probably due to the chemical reaction of $TiC_p$ with B in the matrix.

For the MMC coating with undissolved TiCp reinforcements, interfaces are thermodynamically unstable and have the kinetic possibility to evolve to a more stable configuration due to the high temperature in the molten pool during laser cladding. Chemical reactions to a various degree may occur at phase interfaces. Therefore, the epitaxial growth, precipitation, and chemical reaction are present at the interface of undissolved $TiC_p$. These brittle metallic compounds may impair the mechanical properties and bring about a low-stress failure at the phase interface between $TiC_p$ and the matrix.

In situ MMCs are multiphase materials whose reinforcing phases are synthesized in a metallic matrix during their composite fabrication. They offer attractive advantages as compared to the conventional MMCs: (1) the in situ formed reinforcements are thermodynamically stable in the matrix, leading to less degradation in high temperature; (2) the reinforcement-matrix interfaces are clean, contributing to an improve-

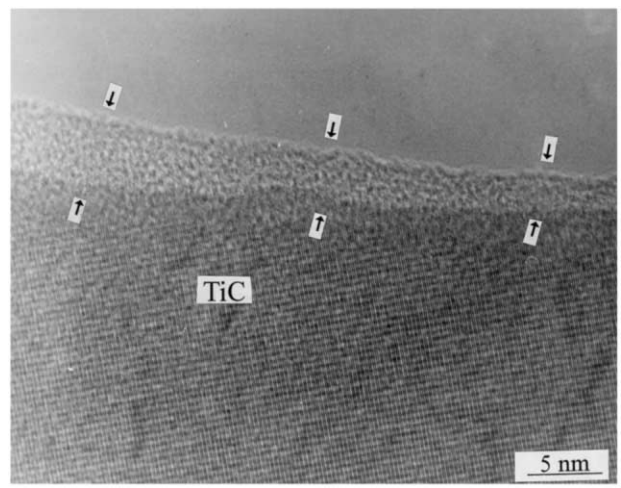


Fig. 4. HRTEM micrograph showing a chemical reaction layer around the phase interface of undissolved $TiC_p$.

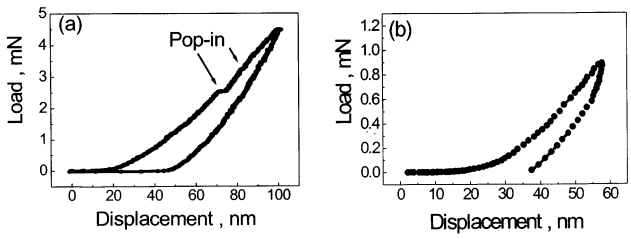


Fig. 5. Load-displacement curve near the $TiC_p$ interface. (a) undissolved $TiC_p$, (b) in situ reacted $TiC_p$.

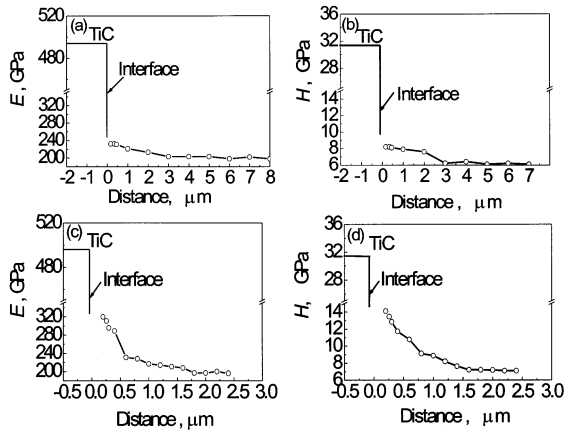


Fig. 6. Distribution of modulus ($E$) and hardness ($H$) near the phase interface. (a), (b) Undissolved $TiC_p$ (c), (d) in situ reacted $TiC_p$.

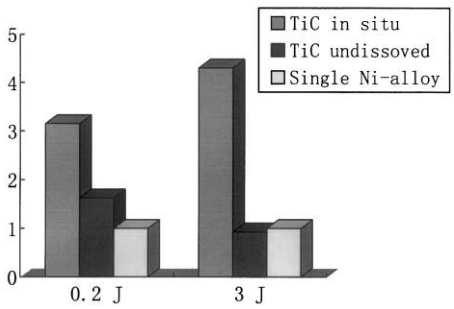


Fig. 7. Relative wear resistance of various coatings after the impact work of 0.2 and 3 J, respectively.

ment of wettability; (3) the in situ formed reinforcing particles are finer in size and their distribution is more uniform, resulting in better mechanical properties of the MMCs. As for in situ reacted $TiC_p$, therefore, the phase interface is clean and free from gas absorption, oxidation or other deleterious surface reactions [16]. This is considered to be one of main advantages of in situ generated interfaces.

### 3.2. Distribution of hardness and modulus

Fig. 5 is the representative load-displacement curve in the matrix region very near the $TiC_p$–matrix interface. Fig. 5(a) and (b) correspond to undissolved and in situ reacted $TiC_p$, respectively. The indent distance from the interface is about 200 and 120 nm, respectively. Fig. 5(a) shows clearly several pop-in marks, with the displacement from a few to tens of nanometers, right from the beginning of loading during indentation even at a very low load. In addition, as for undissolved $TiC_p$, it is noted that the pop-in park appears throughout the loading curve with various loads. However, no pop-in marks appear in Fig. 5(b) in case of the in situ reacted $TiC_p$.

Pop-in marks in the loading curve predict either onset of plastic deformation of crack formation or $TiC_p$ debonding from the matrix. Pop-in phenomenon, in fact, represents the fracture toughness, i.e. resistance to crack initiation and propagation near the $TiC_p$–matrix interface. Thus, the pop-in mark may have resulted from the low fracture toughness. As far as in situ reacted $TiC_p$ is concerned (Fig. 5(b)), however, no pop-in marks appear during loading over a wide range. This suggests that there is no formation of cracks or debonding of $TiC_p$ from the matrix. The interfacial microstructure has a strong influence upon the fracture toughness. The formation of brittle compounds due to precipitation and chemical reaction at interfaces adversely affects the fracture toughness and leads to a low stress fracture. Therefore, it is concluded that the phase interface of in situ generated $TiC_p$ has higher fracture toughness than that in the case of undissolved $TiC_p$.

Fig. 6 reveals the distribution of $E$ and $H$ at matrix regions near phase interfaces corresponding to undessolved and in situ generated $TiC_p$, respectively. $E$ and $H$ all have a gradient distribution. However, it is noted that the in situ generated $TiC_p$ gives values of $E$ and $H$ much higher than undissolved $TiC_p$ does. This means that in situ reacted $TiC_p$ may effectively enhance the hardness and modulus of the matrix and decrease the stress concentration near the interface.

In situ generated $TiC_p$ is introduced into the metal matrix by a direct reaction. It may be more compatible with the matrix and the phase interfaces may be clean [16]. Meanwhile, $TiC_p$ formed in situ is ultra-fine and thermally stable [16,17]. Therefore, $TiC_p$ generated in situ can increase $E$ and $H$ effectively.

The results provided useful information that in situ reacted $TiC_p$ has a higher stiffness and a better combination of strength and toughness than those of undissolved $TiC_p$ do.

### 3.3. Impact wear resistance

Fig. 7 shows the relative wear resistance. The relative wear resistance is determined by calculating the ratio of the measured weight change of the single Ni-alloy coating to that of coatings with $TiC_p$. Under the conditions of both low (0.2 J) and high (3 J) impact work,

the coating reinforced by in situ reacted $TiC_p$ has the best wear resistance, as compared with the coating reinforced by undissolved $TiC_p$ and the single Ni-alloy coating. As for the coating reinforced by undissolved $TiC_p$, the wear resistance increases at the low impact work but decreases at the high impact work, as compared with the single Ni-alloy coating.

The morphologies of the worn surface after impact work of 3 J are showing in Fig. 8. For the coating reinforced by in situ reacted $TiC_p$ (Fig. 8(a)), only mild adhesive wear with fine scratches appears. For the coating reinforced by undissolved $TiC_p$ shown in Fig. 8(b), however, both the severe delamination wear of large areas and the desquamation of a large amount of $TiC_p$ from matrix occur. In addition, microcracks form next to the existing defects or the drastic plastic deformation zones in the subsurface layers. Thus, the impact wear mechanism is the sequence of nucleation and propagation of microcracks at phase interfaces, and then debonding of carbide from the matrix in the present coating.

Basically, to improve effectively the impact wear, surface and subsurface plastic deformation, crack initiation, and crack growth should be reduced [13]. The onset of microcracking depends on the fracture toughness. The wear resistance will be enhanced with an increase in fracture toughness when microcracking becomes the predominant wear mechanism. The delamination wear mechanism is less load dependent, being mainly a function of the number of defects in the materials [18]. Plastic deformation during wear causes dislocation pile-ups in the subsurface layers leading to the formation of microcracks followed by delamination. In addition, the desquamation of $TiC_p$ from matrix is mainly determined by the fracture toughness of the interface between $TiC_p$ and the matrix.

The fine $TiC_p$ reacted in situ enhances the fracture toughness of not only the phase interface but also the bulk coating. The gradient distribution of hardness may also alleviate the stress localization near interfaces. Meanwhile, finely and dispersely distributed $TiC_p$ particles reacted in situ may effectively restrain the deformation of the ductile matrix. This means that the in situ $TiC_p$ coating possesses a much higher resistance to plastic deformation and microcracking and as a result, an enhanced resistance to debonding of particles from the matrix. The phase interface of undissolved $TiC_p$ presents various precipitates. The phase interface has a low fracture roughness and as a result, microcracks easily form especially at a high impact load. This is why the coating has a poor wear resistance at a high impact work, as compared with the single Ni-alloy coating.

Therefore, under the present wear condition, it is expected that a large amount of fine, disperse and well-distributed in situ $TiC_p$ particles with a strong interface bond will be sure to enhance the wear properties of the layer effectively.

## 4. Conclusions

The phase interfaces between $TiC_p$ and the matrix are studied by ATEM and HRTEM in a Ni-alloy coating reinforced by $TiC_p$. The epitaxial growth of TiC, precipitation of CrB and $M_{23}C_6$ compound, and chemical reaction layer are observed.

$TiC_p$ generated in situ leads to a high toughness, hardness, and modulus than undissolved $TiC_p$ does. For $TiC_p$ undissolved, pop-in phenomenon can be seen in the load-displacement curve. Pop-in marks result from onset of plastic deformation from the crack formation or debonding of particle from the matrix.

The coating reinforced by $TiC_p$ reacted in situ has the best impact wear resistance at both low and high impact work. The coating reinforced by undissolved $TiC_p$ has a high wear resistance only at low impact work but not at high impact work, as compared with the Ni alloy coating without $TiC_p$. The degree of wear for the composite coating depends primarily on the debonding removal of $TiC_p$.

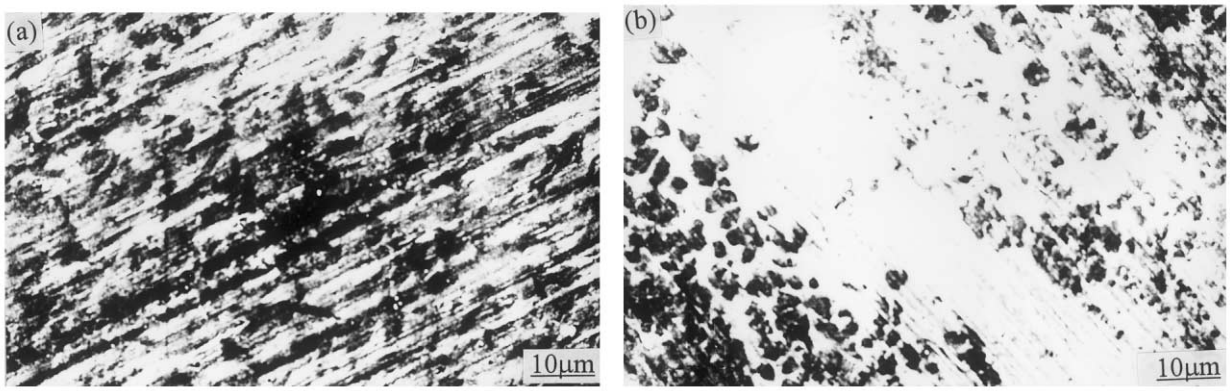


Fig. 8. SEM micrographs of worn surface after the impact work of 3 J. (a) In situ reacted $TiC_p$, (b) undissolved $TiC_p$.

## Acknowledgements

This research was supported by National Natural Science Foundation (Grant No.19891180), National Outstanding Youth Scientific Award of China (Grant No.19525205) and The Chinese Academy of Sciences.

## References

[1] W. Cerri, R. Martinnella, G.P. Mor, Surf. Coat Technol. 49 (1991) 40–45.
[2] P. Molian, H. Rajasekhara, Wear 114 (1987) 19.
[3] S.J. Matthews, in: E.A. Metzbower, S.M. Copler (Eds.), Applications of Lasers in Materials Processing, ASM, Metals Park, OH, 1983, p. 138.
[4] G. Abbas, D.R.F. West, Wear 143 (1991) 353.
[5] J.D. Ayers, R.J. Schaefer, W.P. Robey, J. Met. 8 (1981) 19.
[6] J.D. Ayers, T.R. Tuoker, R.C. Bowers, Scripta Metall. 14 (1980) 549.
[7] T.C. Lei, J.H. Ouyang, Y.T. Pei, Y. Zhou, Mater. Sci. Technol. 11 (1995) 520.
[8] K.M. Jasim, R.D. Rawlings, D.R.F. West, J. Mater. Sci. 28 (1993) 1820.
[9] J.H. Abboud, R.D. Rawlings, D.R.F. West, Mater. Sci. Technol. 10 (1994) 414.
[10] M. Boas, M. Bamberger, G. Revez, Surf. Coat Technol. 42 (1990) 175.
[11] K.P. Kooper, J.D. Ayers, Surf. Eng. 1 (1985) 263.
[12] X.B. Zhou, P.M. Bronssveld, J. Hosson, Lasers Eng. 1 (1991) 145.
[13] T. Weissenberg, J. Wiedemeyer, Wear 130 (1989) 275.
[14] W.C. Oliver, G.M. Pharr, J. Mater. Res. 7 (1992) 1564.
[15] D.B. Marshall, W.C. Oliver, J. Am. Ceram. Soc. 70 (1987) 542.
[16] X.L. Wu, J. Mater. Res. 14 (1999) 2704.
[17] X.L. Wu, Surf. Coat Technol. 115 (1999) 111.
[18] S.C. Lim, M.F. Ashby, Acta Metall. 35 (1987) 1.